# Calculations of safe collimator settings and $\beta^*$ at the CERN Large Hadron Collider

R. Bruce,* R. W. Assmann,† and S. Redaelli
*CERN, Geneva, Switzerland*
(Received 18 February 2015; published 22 June 2015)

The first run of the Large Hadron Collider (LHC) at CERN was very successful and resulted in important physics discoveries. One way of increasing the luminosity in a collider, which gave a very significant contribution to the LHC performance in the first run and can be used even if the beam intensity cannot be increased, is to decrease the transverse beam size at the interaction points by reducing the optical function $\beta^*$. However, when doing so, the beam becomes larger in the final focusing system, which could expose its aperture to beam losses. For the LHC, which is designed to store beams with a total energy of 362 MJ, this is critical, since the loss of even a small fraction of the beam could cause a magnet quench or even damage. Therefore, the machine aperture has to be protected by the collimation system. The settings of the collimators constrain the maximum beam size that can be tolerated and therefore impose a lower limit on $\beta^*$. In this paper, we present calculations to determine safe collimator settings and the resulting limit on $\beta^*$, based on available aperture and operational stability of the machine. Our model was used to determine the LHC configurations in 2011 and 2012 and it was found that $\beta^*$ could be decreased significantly compared to the conservative model used in 2010. The gain in luminosity resulting from the decreased margins between collimators was more than a factor 2, and a further contribution from the use of realistic aperture estimates based on measurements was almost as large. This has played an essential role in the rapid and successful accumulation of experimental data in the LHC.

DOI: 10.1103/PhysRevSTAB.18.061001 PACS numbers: 29.20.db, 29.27.-a

## I. INTRODUCTION

During the design and operation of a collider, such as the Large Hadron Collider (LHC) [1,2] at CERN, it is essential to maximize the accumulated data at the experiments and thus the time integral of the luminosity $\mathcal{L}$. As usual, we define luminosity as the event rate per unit cross section. The instantaneous luminosity for round beams and optics can be written as [3]

$$\mathcal{L} = \frac{N_1 N_2 f_{\mathrm{rev}} k_B}{4\pi\beta^* \epsilon_{xy}} \times F, \tag{1}$$

where $\beta^*$ is the optical $\beta$-function at the collision points in both transverse planes, $N_i$ is the intensity in beam $i$, $f_{\mathrm{rev}}$ the revolution frequency, $k_B$ the number of bunches per beam, $\epsilon_{xy}$ the geometrical emittance and $F$ a geometric reduction factor, which depends on the crossing angle, the transverse beam size, and the bunch length. Apart from a weak dependence of $F$ on $\beta^*$, $\mathcal{L}$ is inversely proportional to $\beta^*$, meaning that it is desirable to operate with $\beta^*$ as low as possible in order to maximize $\mathcal{L}$ [4].

Around the interaction point (IP) in a collider, there is usually a drift space without magnetic elements, where the experimental detector is located. In the drift, the $\beta$-function at a distance $s$ from the IP is $\beta(s) = \beta^*(1 + s^2/\beta^{*2})$ [3]. It follows that, for $s \gg \beta^*$, the maximum of the $\beta$-function in the drift is approximately inversely proportional to $\beta^*$ and increases when $\beta^*$ is decreased. The effective maximum of the $\beta$-function occurs usually in the quadrupoles in the final focusing system [5], grouped in triplets in the case of the LHC, but is still approximately inversely proportional to $\beta^*$. As an example of a collision point optics, Fig. 1 shows the $\beta$-functions used in 2012 around the ATLAS experiment in the LHC together with the lattice [6]. The optics around CMS is similar except that the horizontal and vertical planes are swapped. The setup is conceptually similar to an optical system, where a wide beam of light is focused down in a point by a focusing lens followed by a drift space.

If the beam size increases in the elements close to the IP, the beam tails come closer to the aperture, especially at the peak of the $\beta$-function, which for the LHC is in the inner triplets in the final focusing system (see Fig. 1). For a sufficiently small $\beta^*$, the triplets become the limiting aperture bottlenecks of the machine, which leads to an increased risk of local beam losses. For the LHC, which is designed to store a total beam energy of 362 MJ, this is critical. The local loss of a very small fraction of the full beam can cause enough heat deposition for a magnet to

*roderik.bruce@cern.ch
†Present address: DESY, Hamburg, Germany.

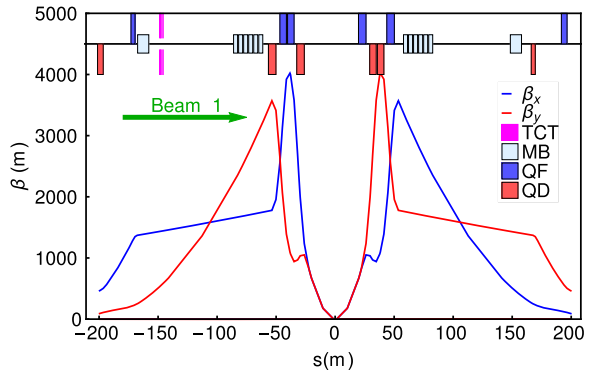


FIG. 1. The $\beta$-functions around the ATLAS experiment in the LHC for the clockwise rotating beam (B1), calculated with MAD-X [7], shown together with the layout of dipoles (MB, main bend), horizontally focusing (QF) and defocusing (QD) quadrupoles, and tungsten collimators (TCTs) for protection of the aperture bottleneck. This optics [6] with $\beta^* = 60$ cm was used in the 2012 physics run. The IP is located at $s = 0$ and the beam direction is from left to right, meaning that the incoming beam passes the TCTs before the inner triplets and the IP. The optics is identical in CMS except that the horizontal and vertical planes are switched.

pass from a superconducting to a resistive state (a quench) or even induce material damage.

To prevent such losses, a collimation system has been installed [2,8–13]. However, the triplet aperture can only be protected if the distance between the aperture and the central beam orbit, in units of the local RMS beam size $\sigma$, is larger than the cut made by the collimators. If the $\beta$-function in the triplet becomes sufficiently large, this is no longer the case, unless the collimators are moved in. Therefore, the collimation system imposes a limit on the maximum allowed $\beta$-function in the triplet and also on the minimum $\beta^*$ [14]. Consequently, an optimization of the collimator settings can push this limit and thus also the luminosity performance.

In this article, we show methods to calculate collimator settings that maximize the performance without compromising machine protection. As application we use the 2012 LHC physics run, however, the methods could be adapted to any circular collider where the stored beam energy is high enough to cause damage and fast failure modes exist. This includes the future high-luminosity LHC (HL-LHC) [15] and the Future Circular Collider (FCC) [16].

We give a brief overview in Sec. II of the LHC and its collimation system, as well as the performance evolution in the first LHC running period 2010–2013, called Run I. After that, we show in Secs. III–IV how optimal LHC collimator settings have been determined for different collimator types. The focus is on protecting sensitive machine elements from fast beam failures, although we shortly discuss also considerations for losses during standard operation. Section V discusses the calculation of the aperture margin as a function of $\beta^*$ and Sec. VI shows the resulting reach in $\beta^*$. In Sec. VII we examine, using numerical simulations, the influence of various approximations used in the calculations, and Sec. VIII gives an outlook toward future LHC running scenarios. All abbreviations used in the text are summarized in Appendix A

It should be noted that, for proton operation, our discussion applies mainly to the high-luminosity experiments in the LHC (ATLAS and CMS) with colliding beams at top energy (called stable beams). The other LHC experiments are limited in event rate and do not gain from an increased peak luminosity. During other phases of the machine cycle such as injection and energy ramp, there is no incentive to operate at a small $\beta^*$ and the margins can thus be relaxed. Similar constraints apply to the operation with heavy ions, where in addition the ALICE experiment can profit from a small $\beta^*$.

## II. THE LHC AND ITS COLLIMATION SYSTEM

### A. LHC in Run I

The main proton beam parameters at the LHC during the first years of operation, as well as the design values, are listed in Table I. Operation started at a beam energy of 3.5 TeV in 2010, which was raised to 4 TeV in 2012, while the aim is to achieve the design energy of 7 TeV in the future. The LHC consists of 8 arcs and 8 straight sections, called insertion regions (IRs) with different functionalities. A schematic layout is shown in Fig. 2. Four of the IRs house interaction points (IPs) where the two counterrotating beams (called B1 and B2) collide inside experiments.

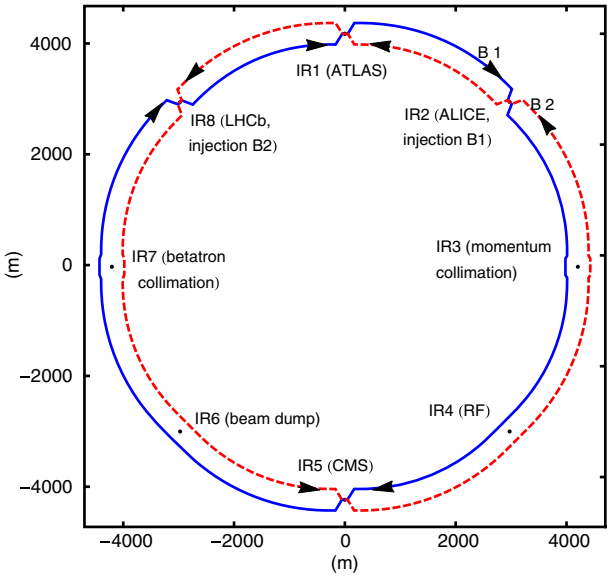


FIG. 2. The schematic layout of the LHC (the separation of the two rings is exaggerated). The two beams are brought into collision at the four experiments ATLAS, ALICE, CMS, and LHCb. Adapted from Ref. [17].

TABLE I. Proton beam parameters for the LHC in nominal collision conditions [2] as well as the parameters used in 2010, 2011, and 2012.

| Operational scenario | 2010 | 2011 | 2012 | Design |
|---|---|---|---|---|
| Proton energy (TeV) | 3.5 | 3.5 | 4 | 7 |
| Max number of bunches per beam | 368 | 1380 | 1380 | 2808 |
| Protons/bunch (average at start of collisions) | $1.0 \times 10^{11}$ | $1.3 \times 10^{11}$ | $1.5 \times 10^{11}$ | $1.15 \times 10^{11}$ |
| Transv. normalized emittance, typical value in collision ($\mu$m) | 2.6 | 2.4 | 2.4 | 3.75 |
| Peak stored energy per beam (MJ) | 23 | 112 | 146 | 362 |
| Horizontal and vertical $\beta^*$ at IP1 and IP5 (m) | 2.0, 3.5 | 1.5, 1.0 | 0.6 | 0.55 |
| Maximum peak luminosity $\mathcal{L}$ at IP1 and IP5 ($\mathrm{cm}^{-2}\,\mathrm{s}^{-1}$) | $2.1 \times 10^{32}$ | $3.5 \times 10^{33}$ | $7.7 \times 10^{33}$ | $10^{34}$ |
| Integral $\int \mathcal{L} dt$ at IP1 and IP5 over the year ($\mathrm{fb}^{-1}$) | 0.048 | 5.5 | 22.8 | — |

Table I shows also the $\beta^*$-values used in the LHC in Run I. At the startup in 2010, the very first operation took place at $\beta^* = 2$ m, but after the machine protection constraints that are described in the following sections were realized, a conservative approach was taken, with relatively open collimator settings and $\beta^* = 3.5$ m and the triplet aperture estimated using pessimistic error tolerances. In 2011, the available aperture was instead assessed based on extrapolations from measurements. Furthermore, the margins between collimator families were for the first time evaluated using our models described in this paper, and it was found that the margins could be significantly reduced without compromising machine protection. As a consequence, $\beta^*$ could in 2011 be decreased to first 1.5 m and later, based on more detailed aperture measurements [18–20] and a tighter normalized beam-beam separation [21,22] to 1 m [23]. For the 2012 run, improvements in our calculation model [24], as well as an empiric reduction of the margins between betatron collimators, made it possible to squeeze $\beta^*$ to 60 cm.

In summary, $\beta^*$ was decreased in steps from 3.5 m to 0.6 m during Run I, which is a gain by a factor 5.8. The dominating contributions came from the tighter collimation margins for machine protection (factor 2.3) and the use of the measured aperture instead of theoretical estimates based on pessimistic tolerances (factor 1.7). The tighter betatron collimator settings contributed by about 30%, the smaller beam-beam separation by 12% and the energy increase from 3.5 TeV to 4 TeV by 4%. It is therefore clear that the tightening of the collimator settings, based on the calculation models presented in this article, have played a key role for the LHC in achieving a $\beta^*$ which is very close to the nominal design value, despite running at about half of the design energy.

### B. LHC collimation

The LHC uses superconducting magnets and stores highly destructive beams with an unprecedented stored energy (see Table I). A local beam loss of a fraction of a few $10^{-9}$ of full the beam might induce a quench and a fraction of a few $10^{-4}$ risks to damage sensitive equipment. To avoid this, a beam loss monitor (BLM) system is in place [25,26] that can trigger a beam dump within 1–3 turns if the losses are too high. The beams are extracted by 15 horizontal kicker magnets, called MKDs, that go from zero to full field in about 3 $\mu$s or 3% of the revolution period [2]. Therefore, all LHC filling schemes contain a series of empty buckets (called abort gap), to which the firing of the MKDs is synchronized.

All beam losses must be tightly controlled in order to avoid beam dumps and costly downtime. Therefore, a multistage collimation system is installed [2,8–13]. Most collimators have two movable jaws, with the beam passing in the center between them. The openings of the collimators are usually expressed in units of the local betatronic RMS beam size [27]

$$\sigma = \sqrt{\beta \epsilon_n / (\beta_{\mathrm{rel}} \gamma_{\mathrm{rel}})}. \tag{2}$$

Here $\beta$ is the nominal optical Twiss function, $\epsilon_n = 3.5$ $\mu$m the nominal normalized transverse emittance [2], and $\beta_{\mathrm{rel}}$ and $\gamma_{\mathrm{rel}}$ are the relativistic parameters. A collimator setting $n$ means that the two jaws are positioned at a transverse distance of $\pm n\sigma$ around the beam center.

The collimators are ordered in families, each set at a different $n$, that have to obey a strict hierarchy to ensure optimal performance. Closest to the beam, in the betatron cleaning insertion IR7, are primary collimators (TCP7), followed by secondary collimators, (TCS7). Both are made of carbon fiber composite (CFC) and robust enough to withstand the impact of several bunches without damage [2]. Further out are tungsten absorbers (TCLA7). There is also a similar but separate hierarchy of momentum collimators in IR3, consisting of TCP3, TCS3, and TCLA3. In the experimental IRs, tertiary collimators (TCTs) made of tungsten provide local protection of the triplets and decrease the experimental background [17]. The TCTs and TCLAs are not robust and should not intercept large beam losses as they otherwise might be damaged [28].

### C. Protection during fast failures

Apart from intercepting beam losses during routine operation, the collimation system must also protect the machine from damage in case of abnormal beam losses that

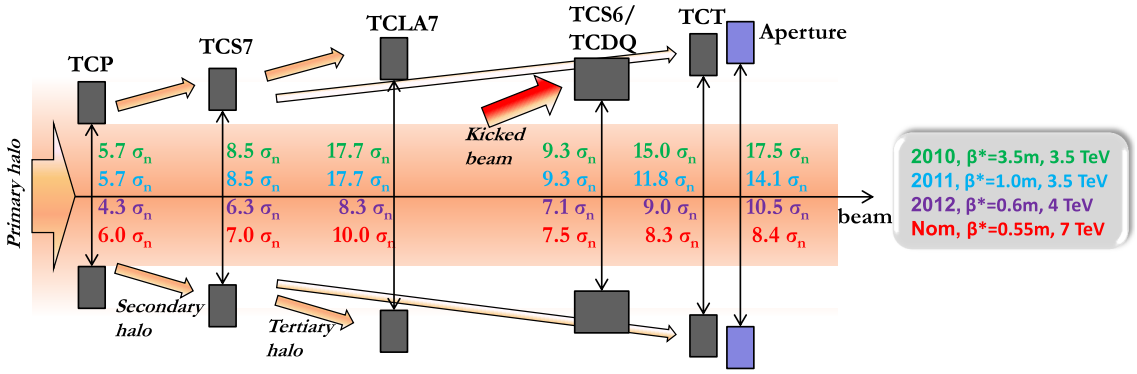


FIG. 3. Schematic illustration (not to scale) of the collimator settings and the minimum aperture that can be protected during the physics runs in 2010 (3.5 TeV), 2011 (3.5 TeV), and 2012 (4 TeV), together with the nominal settings (7 TeV). The resulting values of $\beta^*$ are also indicated.

occur so fast (less than two turns) that the beam cannot be extracted. The main accident scenario is a failure of the beam dumping system itself, where the MKDs erroneously trigger outside the abort gap [2,29–31]. One or several bunches could receive intermediate kicks and be deflected directly onto sensitive equipment and potentially cause damage. This accident, when all MKDs fire simultaneously but at the wrong moment, is called an asynchronous dump (AD). Another failure mode, called single-module pre-fire (SMPF), consists in only one MKD firing. A retriggering system then makes the remaining MKDs fire, but this happens after a delay of about 650 ns. With a SMPF, it takes more time to reach the extraction strength, meaning that more bunches risk to receive intermediate kicks. Therefore, the SMPF is the most serious accident scenario.

To protect against this, special dump protection collimators (called TCS6 and TCDQ) are installed in IR6, directly downstream of the beam extraction [32]. The TCDQ is a one-sided, 6 m long graphite absorber block, designed for maximum robustness. It is supplemented by the TCS6, which is 1 m long, two-sided, and has the same design as the TCS7.

### D. Collimation margins

For the protection to work, the TCDQ must shadow all sensitive equipment that could potentially be damaged, in particular the triplets close to the experiments and all tungsten collimators (TCTs and TCLAs) which are not designed to intercept high losses. Furthermore, the dump protection devices must be at a larger setting than the TCP7s and TCS7s, as they otherwise would intercept primary or secondary beam halo, inducing large losses in an insertion not designed for this. This collimation hierarchy is schematically illustrated in Fig. 3. The last step is the aperture protected by the collimators, which directly imposes a lower limit on $\beta^*$.

The collimators are aligned around the reference orbit one to a few times per year and the protection is qualified with provoked losses at low intensity [13,33,34]. Between alignments, we rely on the machine reproducibility and the collimators are positioned as in the previous alignment. Because of unavoidable drifts over time of the orbit and optics, which brings the beam center closer or farther away from the aperture or collimators in units of $\sigma$, margins are needed in the collimation hierarchy to ensure that the hierarchy holds.

The importance of the margins should be put in relation to what could happen in case of a violation. If a TCS7 would intercept primary halo, the cleaning efficiency risked to drop, possibly causing a beam dump and downtime while the LHC is refilled. Although this should be avoided, it does not imply a risk of damage and it can be corrected if observed frequently (for example by realigning the collimators or increasing the margins). However, a violation of the margins between dump protection, TCTs, and aperture could potentially lead to serious damage of the LHC with several months of downtime for repair. These margins are thus more critical.

Therefore, the problem of finding the limit on $\beta^*$ from collimation constraints can be split in three parts: (i) find the minimum setting of the betatron collimators in IR7 and the IR6 dump protection (ii) find the minimum margins between TCDQ, TCTs, and the aperture compatible with machine protection, and (iii) estimate the aperture margin in $\sigma$ for different configurations of $\beta^*$ and crossing angle in order to conclude on the optimal configuration compatible with the collimators. Although (ii) and (iii) are the main topics in this paper, we briefly describe also (i) in the following section.

## III. DETERMINATION OF COLLIMATOR SETTINGS IN IR7 AND IR6

The primary purpose of the margins in IR7 is to ensure that the hierarchy remains intact for optimal cleaning performance. There are also lower limits on the settings. If the TCP7 are positioned too close to the beam, they risk

scraping significant fractions of the beam core, which has a negative effect on the beam lifetime and consequently on integrated luminosity. Furthermore, if the orbit moves, more beam is scraped off at a tighter setting, possibly resulting in beam dumps. The collimators are also the dominating contribution to the LHC impedance [35] and with smaller gaps, the impedance increases, potentially causing instabilities.

It is very difficult to quantitatively predict the probability of instabilities, with losses high enough to cause beam dumps, as a function of the collimator impedance, especially in the presence of beam-beam effects. If such a model existed, it could be used to evaluate the collimator settings that give the optimum integrated luminosity, in a trade-off between smaller $\beta^*$ and increased number of beam dumps and downtime.

Instead, an empirical approach was used during Run I, also because the drifts in optics and orbit were not known at the start of the run. In 2010 and 2011, the margins between TCP7, TCS7, and IR6 collimators were kept constant in mm after the injection plateau (so-called relaxed collimator settings [12,36]). This larger-than-design retraction allowed operational margins to ensure long-term machine stability. For the 2012 run, both the TCP setting and the IR7 margins were decreased (so-called tight settings) based on experimental studies of the long-term hierarchy stability and impedance [37–40]. This resulted in a gain of $2.2\sigma$ margin, which was an important contribution to the decrease in $\beta^*$ from 1 m to 60 cm in 2012. However, it should be noted that the number of observed instabilities increased significantly in 2012 [41,42]. All Run I settings are summarized in Fig. 3.

## IV. DETERMINATION OF TCT SETTINGS AND ALLOWED APERTURE

### A. Basic assumptions

The margins between IR6 and the TCTs, and between TCTs and aperture, are driven mainly by protection from AD/SMPF. Constraints from cleaning and experimental background are less critical and often satisfied with smaller margins. We therefore focus on the AD/SMPF protection aspect.

In the margins, all effects that could potentially change the distance between an aperture restriction and the beam have to be considered. They are: orbit drifts (both random drifts as well as intentional drifts from luminosity optimization), optics errors, setup errors (inaccuracy of the beam-based collimator alignment), and positioning errors (reproducibility of the collimator position).

These contributions depend on factors that are very hard to predict and control, such as machine imperfections and nonlinearities. Therefore, we use a statistical approach relying on the best available knowledge of the future machine behavior, which in most cases are data from previous runs. For a new or significantly upgraded machine, it is advisable to add additional safety margins. Once the results of our calculations are put into operation, all parameters have to also be studied with beam to verify the assumptions.

Our approach is to first develop a simplified but fast model that can cover a large parameter space and then verify the results using detailed numerical simulations (described in Sec. VII). As application, we calculate the TCT settings and allowed aperture for the 2012 run.

In order to obtain a tractable, semianalytic model, we work in the simplifying assumption that the betatron phase advance from the MKDs to all downstream protection devices and sensitive equipment is an odd multiple of 90°, meaning that a kicked beam is at its maximum excursion. This is approximately true for the TCDQ (94° from the central kicker) while TCTs and triplets have phases at least 30° further away, depending on optics. Since the TCDQ is closer to 90°, our assumption is pessimistic and gives some room for phase advance errors.

We assume also that if a sensitive element is at a larger distance in $\sigma$ than the protection device, it is safe. This assumption, which significantly simplifies the calculations and allows us to picture the protection as a "shadowing" in units of normalized distance to the beam, is not always true. In general, the phase advance could alter this, but with the phases mentioned above our assumption applies to the nominal LHC optics. Furthermore, we neglect that the protection devices are not absorbing all intercepted particles and that a small fraction is outscattered. An additional pessimistic simplification is that we do not include the possible protection by the IR7 collimators. For some TCTs, e.g., in IR5 B2, this is irrelevant, since the beam arrives directly from IR6 without passing IR7 in between. However, IR7 could improve the situation, e.g., for IR1 B1 (see Fig. 2). The IR3 collimators are usually more open and do not contribute to the protection. We assess the influence of all these simplifications through numerical simulations in Sec. VII.

We expect on average one AD or SMPF per beam and year [29]. If $1/3$ of the time is spent in physics operation with colliding beams, and the margin between TCDQ and TCT would be violated less than 1% of the time, we expect less than one AD or SMPF in 150 years with exposed TCTs for any of the two beams. If, in addition, the margin between the TCT and the triplet apertures is violated less than 1% of the time, the event rate exposing the triplet is two orders of magnitude smaller, if the violation of the two margins can be assumed uncorrelated. We consider this risk level acceptable and thus calculate the margins assuming that each device should not be closer to the beam than its upstream protection device more than 1% of the time.

### B. Orbit margins

Since the protection is qualified empirically after the collimator alignment, we need only to account for drifts

occurring afterwards. The distributions of orbit drifts around this reference orbit are extrapolated from previous runs. As an example, measured orbit drifts at a beam position monitor (BPM) close to a TCT are shown in Fig. 4. Data were extracted at 10 s intervals during all periods in 2011 with stable beams. Qualitatively similar orbit distributions are obtained in the triplets. In IR6, smaller systematic offsets but similar spreads are found.

There is a significant spread in the measurements and also a systematic offset for the runs with $\beta^* = 1.0$ m, which is not understood. The drifts are dominated by fill-to-fill variations, while drifts within fills typically have spreads of the order of 50 $\mu$m. Some drifts are believed to be an artifact of temperature-dependent noise of the BPMs, but this is very hard to decouple from real drifts.

To calculate the orbit margins, we consider the measurement results as probability distributions and find the smallest margin $m$, in units of $\sigma$, that cover 99% of all drifts. Since the TCTs and IR6 are far apart with many orbit correctors in between, orbit drifts at these locations are assumed approximately independent, which is also confirmed by the data. Therefore, we calculate the orbit margin $M_{o6T}$ between IR6 and a TCT as

$$M_{o6T} = \sqrt{m_{\mathrm{TCT}}^2 + m_{\mathrm{IR6}}^2}. \tag{3}$$

Equation (3) is evaluated for both beams, and for the TCTs in IR1 and IR5. The final margin, applied to all TCTs, is the maximum over these values.

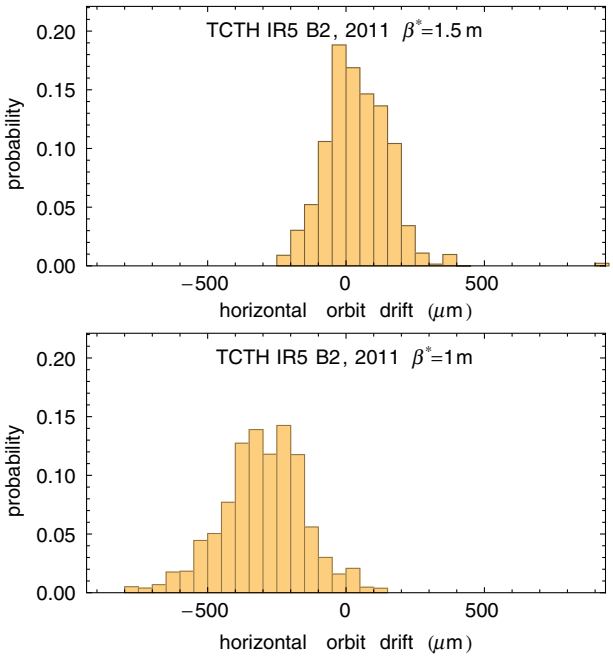


FIG. 4. Measured drifts of the horizontal B2 orbit at a BPM close to the TCTH in IR5 during the first part of the 2011 run with $\beta^* = 1.5$ m (top) and during the second part with $\beta^* = 1.0$ m (bottom). The orbits were sampled every 10 s.

We cannot consider the orbit movements between TCT and triplet as independent, since the elements are close (about 100 m on the incoming beam). Instead, we calculate the margin from the correlated orbit movements. As shown in Appendix B, we can at any given moment calculate the change in margin $\Delta M_{\mathrm{TCT,tr}}$ as

$$\Delta M_{\mathrm{TCT,tr}} = |x_{\mathrm{tr}}| - |x_{\mathrm{tr}} + \Delta x_{\mathrm{tr}} + |\Delta x_{\mathrm{TCT}}||, \tag{4}$$

where $x_{\mathrm{tr}}$ is the triplet reference orbit, and $\Delta x_{\mathrm{tr}}, \Delta x_{\mathrm{TCT}}$ are orbits drifts, all in units of $\sigma$. To calculate the orbit margin $M_{\mathrm{oTT}}$ between TCTs and triplets, we take again the minimum value that covers 99% of the measured $\Delta M_{\mathrm{TCT,tr}}$, and select the maximum over IR1 and IR5 and both beams.

$M_{o6T}$ and $M_{\mathrm{oTT}}$ in the two parts of the 2011 run, and the later achieved values in 2012, are shown in Table II. All margins, in units of $\sigma$, are scaled to 4 TeV as used in 2012. The largest margins are obtained with the 2011 data, which were used to determine the 2012 settings.

We expect orbit drifts to be independent of $\beta^*$ in $\mu$m but not in $\sigma$, since the nearby $\beta$-function varies with $\beta^*$. We could include this scaling in the margin, however, this is not done except for very large changes in $\beta^*$. The reason is that we otherwise could be too optimistic. For example, in Fig. 4 the drifts in $\sigma$ are expected to be smaller by a factor $\sqrt{1/1.5}$ after the change in $\beta^*$. However, due to a systematic shift of the distribution mean, which is not well understood, the drifts in $\sigma$ are instead slightly larger at $\beta^* = 1$ m. The orbit in 2012 with $\beta^* = 0.6$ m shows, however, a scaling with $\beta^*$ as expected (Table II).

Figure 4 makes it clear that one cannot assume to have exactly the same orbit distribution as in the previous machine configuration. However, since we pessimistically use the maximum over two IRs and two beams, and do not include the scaling with $\beta^*$, the calculation is less sensitive to local variations. Indeed, the margin calculated using data from the two parts of the 2011 run with different $\beta^*$ are similar (see Table II).

In addition to the random drifts, there are intentional ones in the IRs when the luminosity is optimized and the beams are scanned transversely. This causes orbit shifts at the triplets and the TCTs. We assume a margin of $0.2\sigma$ for

TABLE II. Margin IR6–TCTs and TCT–triplet in units of $\sigma$, needed to ensure a correct collimation hierarchy during 99% of all observed orbit movements calculated using data sets from different running periods in 2011 and 2012 with $\beta^* = 0.6$ m. The data were sampled every 10 s during all periods with stable beams.

| Data set | $M_{o6T}$ | $M_{\mathrm{oTT}}$ |
|---|---|---|
| 2011, $\beta^* = 1.5$ m ($\sigma$) | 1.2 | 1.2 |
| 2011, $\beta^* = 1.0$ m ($\sigma$) | 1.2 | 1.2 |
| 2012, $\beta^* = 0.6$ m ($\sigma$) | 1.3 | 0.9 |

these scans as calculated in Ref. [43]. This margin $M_{\mathrm{scan}}$ cannot be treated as a random component and is thus added separately.

### C. Margin for $\beta$-beat

The collimator positions during stable beams are calculated using the nominal $\beta$-function, although the real $\beta$-function may be different. The $\beta$-beating has to be accounted for in the margins, since a change in beam size means that aperture restrictions come closer or farther away from the beam center in units of $\sigma$.

We cannot calculate the decrease in margin from $\beta$-beat at all times as for the orbit, as it was not measured continuously but only in dedicated measurements [44–46], which have errors as large as the deviations they are measuring. Therefore, we consider an upper bound $|\beta_r/\beta_d - 1| < 10\%$ at all elements as in the 2011 run [45], where $\beta_r$ is the real $\beta$-function and $\beta_d$ its design value. We then calculate separately the change in effective aperture at different elements, by considering first a collimator at $n\sigma$. We assume that the gap in mm was calculated using $\beta_d$. The actual setting $n_r$ relative to the beam, in units of $\sigma$, is then given by solving

$$n_r\sqrt{\beta_r\epsilon_{xy}} = n\sqrt{\beta_d\epsilon_{xy}}. \tag{5}$$

The change in margin $\Delta M_\beta = n_r - n$ in units of $\sigma$ is

$$\Delta M_\beta = n\left(\sqrt{\frac{\beta_d}{\beta_r}} - 1\right) \tag{6}$$

and use as margin between two elements the square sum of the contributions

$$M_\beta = \sqrt{\Delta M^2_{\beta,1} + \Delta M^2_{\beta,2}}. \tag{7}$$

It should be noted that $M_\beta$ depends only on the $\beta$-beat and the nominal opening of the collimator—the smaller the opening, the smaller the error in $\sigma$.

### D. Setup and positioning errors

There is a possible nonreproducibility of the position to which a collimator returns every fill, which we account for in the margins. This is generally a very small effect but can be significant in some cases, for example after a power cut. We estimate this positioning error to less than 50 $\mu$m, which is typically less than 0.05–0.2$\sigma$.

The collimator alignment is performed by moving in each jaw in steps until the circulating beam is touched and a signal is observed on the downstream BLM [33]. It has a limited precision, given mainly by the step size. It is 10 $\mu$m, except for the TCDQ, which has a different motor type and is limited to about 100 $\mu$m accuracy.

When calculating the total margin between two devices 1 and 2 we add their separate contribution in square. The margin $M_{\mathrm{setup}}$ for setup errors is thus

$$M_{\mathrm{setup}} = \sqrt{M^2_{\mathrm{setup},1} + \Delta M^2_{\mathrm{setup},2}}, \tag{8}$$

with an analogue expression to determine $M_{\mathrm{pos}}$ for positioning errors.

### E. Calculation of total margin

To calculate the total margin between two devices, all errors have to be combined. An example of the different contributions for the TCDQ and the TCTs, as calculated for the 2012 run, is shown in Table III. The dominating error source is the orbit, followed by the $\beta$-beat.

One method for combining the tolerances would be to use the maximum possible error as a margin and thus add the different contributions linearly. This method, used to calculate the settings in the 2011 run, is very safe and gives rather large margins and a higher limit on $\beta^*$. As it is unlikely that all errors would simultaneously assume their maximum values and add in the same direction, and we allow a 1% violation probability, we treat instead the errors as statistically independent by summing them in square. The only exception to this rule is the luminosity scans, which are accounted for at all times and therefore added linearly.

We presume that orbit errors are independent of the $\beta$-beat, since both are subject to independent global and local corrections. For example, measurements show that the residual closed orbit is larger in the experimental IRs than in the arcs [47], due to the fact that the large-aperture triplet BPMs have a lower precision than the BPMs in the rest of the machine, and that the corrector magnets are constrained since they must act on both beams in the region of the common beam pipe. The $\beta$-beat on the other hand is relatively small in the experimental IRs, with measured levels there of below 5% [46]. The positioning and setup errors originate from different sources and are independent both of each other and of the $\beta$-beat and orbit.

TABLE III. Estimated errors in units of $\sigma$ at 4 TeV from various sources at the dump protection in IR6 and the TCTs. The 2012 collimator settings were used to estimate the $\beta$-beat.

| ($\sigma$) | IR6 | TCT |
|---|---|---|
| Orbit | 0.9 | 0.8 |
| Scans | — | 0.2 |
| $\beta$-beat | 0.35 | 0.4 |
| Positioning | 0.08 | 0.05 |
| Setup | 0.02 | 0.01 |

The total margin $M_{\mathrm{tot}}$ between two devices is thus

$$M_{\mathrm{tot}} = M_{\mathrm{scan}} + \sqrt{M_{\beta}^2 + M_{\mathrm{orbit}}^2 + M_{\mathrm{pos}}^2 + M_{\mathrm{setup}}^2}, \quad (9)$$

where all terms include errors at both the protection device and at the device to be protected. Since the $M_{\beta}$ depends itself on the setting, so does $M_{\mathrm{tot}}$. Therefore the final setting $n_b$ of a device $b$, which should be outside device $a$ in the hierarchy, has to be obtained by solving

$$n_b = n_a + M_{\mathrm{tot}}(n_b). \quad (10)$$

Using Eqs. (6), (7), and (9), we obtain

$$n_b = \frac{n_a + M_{\mathrm{scan}} + \sqrt{(n_a^2 b^2 + M_{\mathrm{orbit}}^2 + M_{\mathrm{pos}}^2 + M_{\mathrm{setup}}^2)(1-b^2) + (n_a + M_{\mathrm{scan}})^2 b^2}}{1-b^2} \quad (11)$$

where $b = \sqrt{\beta_d/\beta_r} - 1$. Given the setting of the TCDQ, Eq. (11) can be applied recursively to find first the setting of the TCTs and then the minimum protected aperture. The calculated collimator settings, used during all physics runs in 2012, are shown in Fig. 3. The minimum allowed aperture of $10.5\sigma$ can be used to calculate the $\beta^*$-reach.

It should be noted that if one would scale the contributions from orbit, positioning and setup errors in the experimental IRs with changing $\beta^*$, $n_b$ in Eq. (11) is a function of $\beta^*$. If the required aperture as a function of $\beta^*$ is known, it can be used to simultaneously solve for the settings and $\beta^*$, although the calculations become more involved. As discussed in Sec. IV B, this is usually not done, in order have a safety margin that compensate for unpredictable changes in the distributions.

## V. CALCULATION OF TRIPLET APERTURE

Starting from the minimum allowed aperture margin, we can calculate the smallest value of $\beta^*$ where the triplet aperture is still protected, if we know also the required aperture $A_1$, which we define as the distance between the beam center and the physical aperture in units of $\sigma$, as a function of $\beta^*$. To calculate $A_1$ at a given $\beta^*$, the so-called $n_1$ method [48,49] was used in 2010, as well as during the LHC design phase. It is a theoretical calculation, where the worst-case value of $A_1$ is determined using the combination of several error sources. In 2010, very conservative tolerances were assumed. However, beam-based aperture measurements [18,20,50–55] have allowed us to reduce the applied errors significantly [19], which has also played a very important role in the reduction of $\beta^*$.

From 2011 and onward, in order to have a fast and realistic evaluation of $A_1$, which can be incorporated in the analytic calculations of collimator settings and $\beta^*$, we use a direct scaling of the measured apertures, which has been shown to be in excellent agreement with the $n_1$ method if realistic tolerances are used [56]. The minimum aperture margin over the 2D transverse cross section is, with the nominal LHC optics [6], usually found very close to the horizontal or vertical axis. Therefore, we use a 1D scaling, taking into account the change in beam size and orbit. We use subscript $o$ at the old, known machine configuration, where the aperture was measured, and $f$ at a future, new configuration. Since the physical aperture in m at the bottleneck is constant, it must hold that

$$|u_{\mathrm{o}}| + A_{\mathrm{o}}\sigma_{\mathrm{o}} = |u_{\mathrm{f}}| + A_{\mathrm{f}}\sigma_{\mathrm{f}}, \quad (12)$$

where $u$ is the transverse orbit extension in the limiting plane at the aperture bottleneck (we use $|u|$ to account for negative orbits), and $A_{\mathrm{o}}$ the measured normalized aperture. Solving Eq. (12) for $A_{\mathrm{f}}$ and replacing the beam size using Eq. (2) with $\beta_{\mathrm{rel}} \approx 1$, we get

$$A_{\mathrm{f}} = A_{\mathrm{o}}\sqrt{\frac{\beta_{\mathrm{tr}}(\beta_{\mathrm{o}}^*)\gamma_{\mathrm{rel,f}}}{\beta_{\mathrm{tr}}(\beta_{\mathrm{f}}^*)\gamma_{\mathrm{rel,o}}}} + \frac{|u(\beta_{\mathrm{o}}^*)| - |u(\beta_{\mathrm{f}}^*)|}{\sqrt{\epsilon_n \beta_{\mathrm{tr}}(\beta_{\mathrm{f}}^*)/\gamma_{\mathrm{rel,f}}}}. \quad (13)$$

In the triplet, we have indicated that both the $\beta$-function $\beta_{\mathrm{tr}}$ and $u$ can be calculated analytically as a function of $\beta^*$ through a scaling from a known configuration, where the full optics functions have been evaluated using, e.g., MAD-X. $\beta_{\mathrm{tr}}$ scales approximately as $1/\sqrt{\beta^*}$, and $u$ is proportional to the required half crossing angle $\phi$, which varies with $\beta^*$ as [57,58]

$$\phi = \frac{d}{2}\sqrt{\frac{\epsilon_n}{\beta^*\gamma_{\mathrm{rel}}}}. \quad (14)$$

Here we assume that the normalized beam-beam separation $d$ is given as input from separate dedicated studies, such as Refs. [21,22]. It should be noted that we can use the real normalized emittance, even if the design value of $\epsilon_n$ is used in Eq. (2) to position the collimators.

Equation (13), with $\phi$ given by Eq. (14), can therefore be used for an analytic evaluation of the aperture, without the need of calculating the optics in the whole ring. Our method has the advantage of being very fast and removes some uncertainties in the error tolerances, since it starts from a measurement.

One could add tolerances in Eq. (13) to the orbit shift and the $\beta$-function, which was done for the 2011 run [43], due to the uncertainty in the future correction. However, later

experience from Run I shows that Eq. (13) gives accurate results without these tolerances [20] and we thus omit them, assuming that the correction will not be worse in the future. This has to be verified with beam before high-intensity operation is allowed and if a worse-than-expected aperture is found, $\beta^*$ has to be increased.

## VI. MINIMUM $\beta^*$ IN THE 2012 RUN

As an example application, we calculate $A_1$ as function of $\beta^*$ for the 2012 run. We take $A_0$ in Eq. (13) as input from the most conservative aperture measurements in 2011 [20], which resulted in a $14\sigma$ aperture at $\beta^* = 1$ m and $\phi = 120$ $\mu$rad. Using this value, Fig. 5 shows $A_1$ as a function of $\beta^*$ for a few different values of $d$. As $d$ is constant, $\phi$ varies along the curves. To calculate $\phi$, we use either $\epsilon_n = 3.75$ $\mu$m, assumed at the design stage, or the more realistic $\epsilon_n = 2.5$ $\mu$m which was achieved in the 2011 run. We use this latter value to determine the $\beta^*$-reach, since there is a gain in using the real emittance.

The LHC beam lifetime at different $d$ was studied experimentally in 2011 [21,22]. Based on these studies, $d = 9.3\sigma_r$ was successfully introduced in the last part of the 2011 run, where $\sigma_r$ is the transverse RMS size of the real beam, as opposed to the design beam size $\sigma$. We thus assume $d = 9.3\sigma_r$ as input also for 2012. This value would have to be adjusted if the bunch intensity would change significantly or if another bunch spacing than 50 ns is used.

To conclude on the optimal $\beta^*$ for 2012, we thus study the curve for $d = 9.3\sigma_r$ and $\epsilon_n = 2.5$ $\mu$m in Fig. 5 (solid line). It crosses the line of the protected aperture from the collimators at $\beta^* = 58$ cm, which can also be calculated analytically by setting $A_1 = 10.5\sigma$ in Eq. (13) and solving for $\beta^*$. Since the aperture measurements have an uncertainty of about $0.5\sigma$, this value was rounded upwards to $\beta^* = 60$ cm, corresponding to $\phi = 145$ $\mu$rad.

This configuration was successfully used during the whole physics run in 2012. Before allowing high-intensity operation, the aperture was measured with beam [20,52] at $\beta^* = 60$ cm, which confirmed our calculated aperture within the measurement error.

## VII. NUMERICAL STUDIES

The calculation model described above relies on the simplifying assumptions of 90° phase advance, no out-scattering, and does not include the protection from other collimators in IR7 and IR3. In order to reduce the uncertainties, we validate the protection through numerical studies that do not rely on these approximations. We show two different numerical methods with different advantages. We simulate the SMPF, as it is more critical than the AD.

### A. Phase space integration

To see the effect of the phase advance on the impacts on different TCTs during a dump accident, we study first the normalized betatron phase space $(X_0, P_0)$ of one bunch at a misfiring MKD, where it receives a normalized kick $\theta$. Using linear optics, $(X_0, P_0)$ can be propagated to any downstream position where they assume the values $(X_i, P_i)$. The condition that a particle is outside the aperture $A_i$ at location $i$ can then be written as:

$$|X_i| \geq A_i \Leftrightarrow |C_{0i}X_0 + S_{0i}P_0 + S_{0i}\theta + D_i\delta| \geq A_i. \quad (15)$$

Here $(C_{0i}, S_{0i})$ are the transfer matrix elements from 0 to $i$, $D_i$ the periodic dispersion at $i$ and $\delta$ the fractional momentum deviation.

The inequality (15) defines a region $R_i$ in the initial phase space at the MKDs. Figure 6 illustrates $R_i$ for the dump protection and the TCTHs for the two beams and for $\delta = 0$ in the horizontal phase space. In this example,

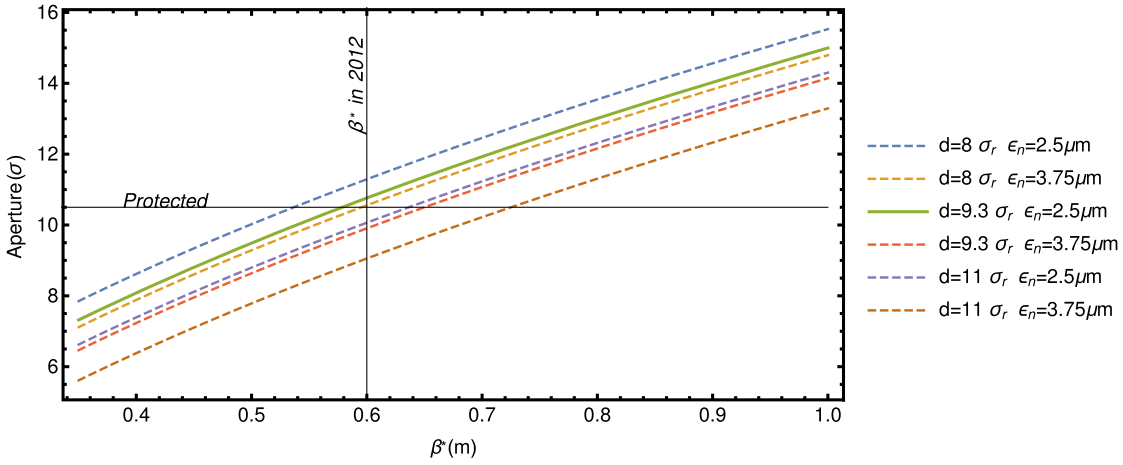


FIG. 5. Calculated triplet aperture, for 4 TeV proton beams with 3.5 $\mu$m in the LHC, as a function of $\beta^*$ for different values of the beam-beam separation $d$, where $d = 9.3\sigma_r$ with the assumption of $\epsilon_n = 2.5$ $\mu$m, was used in LHC operation during the last part of Run I. The calculation was carried out based on Eq. (13) and the measured aperture in 2011. The crossing angle varies along the curves.

$\theta = 7.1\sigma$, meaning that half of the bunch is intercepted by the TCS6, which is positioned at $7.1\sigma$. The approximately horizontal cuts of the TCS6 and the TCDQ show that these collimators are about 90° downstream of the MKDs. Furthermore, the TCTs have for illustrative purposes also been put at $7.1\sigma$. The concentric rings in Fig. 6 show contour lines of the beam distribution $\rho$ at multiples of $\sigma$.

As can be seen in Fig. 6, the TCT most exposed to primary beam during a SMPF is in IR1 B1. It is also the TCT with a phase advance from the MKD closest to an odd multiple of 90° (55°). The TCT in IR5, B2, has a phase advance from the MKD which is very close to a multiple of 180°, and it is therefore not possible to hit it directly with primary beam during a SMPF.

If outscattering is neglected, the particles that are lost on an aperture restriction $i$ are the ones populating the phase space area which is outside the aperture cuts (thus inside $R_i$) but inside all upstream aperture limitations. We denote these regions as the complements $R^c$. Analogue to the method used in Ref. [59], the fraction of a bunch $f_i$ hitting an aperture limit $A_i$ can be calculated by integrating $\rho$ over this phase space area:

$$f_i = \iiint_{R_i \cap R_{i-1}^c \cap \ldots \cap R_1^c} \rho(X_0, P_0, \delta) \mathrm{d}X_0 \mathrm{d}P_0 \mathrm{d}\delta. \quad (16)$$

In order to calculate the leakage fraction, we assume furthermore that $\rho$ is Gaussian:

$$\rho(X_0, P_0, \delta) = \frac{1}{2\pi\sigma^2} \exp\left(-\frac{X_0^2 + P_0^2}{2\sigma^2}\right) \times \frac{1}{\sqrt{2\pi}\sigma_\delta} \exp\left(-\frac{\delta^2}{2\sigma_\delta^2}\right). \quad (17)$$

We call this method phase-space integration (PSI) and use *Mathematica* [60] to evaluate the integrals numerically.

### B. SixTrack

Another method to numerically assess the impacts during a SMPF, which accounts for both the true phase advance, the particle-matter interaction inside collimators, the full ring aperture, and all collimators, is to perform a simulation with the SixTrack code [61–65]. SixTrack does a thin-lens element-by-element tracking through the magnetic lattice, and it has a built-in Monte Carlo code to simulate the particle-matter interaction inside collimators. The particle trajectories are checked against a detailed aperture model with 10 cm longitudinal precision and the simulation output contains coordinates of all loss locations. SixTrack is routinely used to simulate the cleaning performance of the LHC collimation system and the results have been shown to be in very good agreement with beam loss data from the LHC [65].

SixTrack has been adapted to dynamically simulate the firing of one or several MKDs [66,67]. For our studies, an initially Gaussian bunch of macroparticles is tracked for 3 turns, and when the particles pass the MKDs at the second turn, they receive an intermediate kick as during a SMPF. On the third turn, the MKDs have reached their maximum strength that any remaining particles are extracted. This simulation setup has the obvious advantage that it does not rely on any of the assumptions in the semianalytic model but it is limited in precision by the number of tracked macroparticles and requires many orders of magnitude more computing time than the PSI.

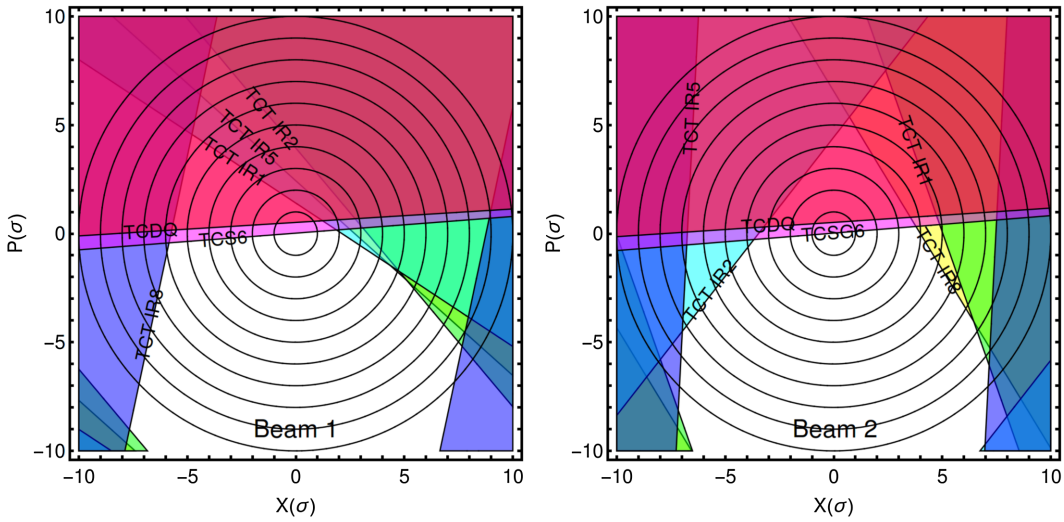


FIG. 6. Example of the on-momentum integration regions defined by Eq. (15) for the dump protection collimators (TCS6 and TCDQ) and all TCTs in B1 (left) and B2 (right) for a setting of $7.1\sigma$ for the TCS6 and the TCTs, while the TCDQ is positioned at $7.6\sigma$. The normalized kick $\theta$ is also at $7.1\sigma$ and a perfect machine is assumed. The circles represent lines of constant phase space density at every $\sigma$. The TCDQ is the first collimator seen by the beam, followed by the TCS6 and the TCTs. A perfect optics and $\beta^* = 60$ cm was assumed.

### C. Results

Using both SixTrack and PSI, we perform one simulation for each 4 TeV bunch in a train with a 50 ns spacing, where every bunch receives a different intermediate kick from each MKD according to the estimated rise of the magnetic field and the retriggering time of adjacent kickers [68]. We use the optics with $\beta^* = 60$ cm and assume $\epsilon_n = 3.5$ $\mu$m. In the end, the simulated losses at each TCT are summed over all bunches.

In order to estimate the sensitivity of TCT losses to the presence of errors, we perform a scan in TCT setting, while keeping all other collimators constant at the 2012 settings shown in Fig. 3. The resulting total TCT losses during a SMPF, as function of the TCT setting, are shown in Fig. 7 for different TCTs, together with estimates of different damage levels [28]. The triplet aperture is kept at its nominal value, and no significant losses are observed there in any simulation. However, because of the almost zero phase advance between TCT and triplet, we expect that the losses in Fig. 7 would move to the triplet if it instead would be the limiting aperture in the IR.

As can be seen, all TCTs are estimated to receive losses below damage onset even if they would be at the level of the TCS6. For low TCT settings, the most critical TCT is in B1, IR1. For this case, SixTrack is in excellent agreement with PSI. For the second most exposed TCT, in IR5 B2, SixTrack shows an approximately constant loss level independently of the opening, while PSI does not show any losses at all. The reason is that the losses in SixTrack are caused by secondary halo with a very flat distribution, i.e., particles that have already hit an upstream collimator, predominantly the TCS6, and have then been outscattered before impacting on the TCT. No losses are seen with PSI since the phase advance between the dump kicker and this TCT is close to 180 degrees (see Fig. 6) so that direct impacts of the primary beam are not possible. These losses on the TCT in IR5 B2 demonstrate that for a complete treatment, we have to include the effect of the outscattering, as done in SixTrack but not in PSI. Secondary halo explains also why the SixTrack losses on the TCT in IR1, B2 are much higher than observed with PSI.

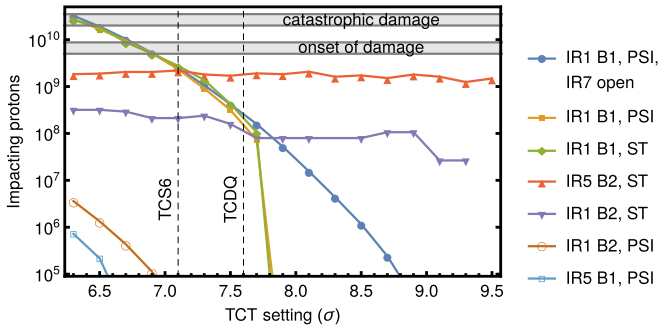


FIG. 7. The simulated losses during a single-module prefire, from PSI and SixTrack (ST), on TCTs in different IRs and beams for 4 TeV 50 ns operation with $\beta^* = 60$ cm optics. Losses are summed over all bunches in a train and shown as a function of the TCT setting. The results are shown together with estimates of the TCT damage limits from Ref. [28].

On the other hand, PSI shows minor losses on the TCT in IR5, B1, where SixTrack does not detect any losses. This is caused by limited precision, and they cannot be detected by SixTrack unless a larger number of macroparticles is simulated—the SixTrack resolution of the results in Fig. 7 is about $2 \times 10^7$ protons. Our results demonstrate the advantages of each method: apart from the much longer computing time, SixTrack is able to simulate the secondary halo but has limited precision. In the range where the impacts are dominated by the primary beam, PSI and SixTrack are in excellent agreement.

In Fig. 7, we show two damage limits, calculated in Ref. [28]. The lower one is for onset of plastic deformations of the material. With this type of damage, the collimator jaw could possibly still be usable, and if not, the collimator can be replaced, resulting in a few days of LHC downtime. Clearly this should be avoided, but the impact on LHC operation is not catastrophic and the risk might be acceptable if it comes with a significant performance increase. At the upper limit, tungsten fragments start detaching from the jaw. Apart from necessitating a collimator replacement, the impact is also a large risk to pollute the vacuum chamber of downstream elements. This scenario would cause a very significant downtime of the LHC and should be avoided.

Figure 7 shows also the influence of the IR7 collimators—the dark blue curve shows, for comparison, the calculated losses from PSI on the IR1 TCT in B1 with all IR7 collimators open. At small TCT openings, the results with and without IR7 collimators agree within 20%, but above a certain TCT setting, IR7 blocks all losses. From SixTrack results (not shown in Fig. 7) it is also clear that, without the IR7 collimators, the IR1 TCT would intercept a significant amount of secondary halo.

It should be noted that the damage limits in Ref. [28] were calculated for a single bunch with nominal emittance at 7 TeV. As our results concern 4 TeV, and the scaling with energy is nontrivial, we have indicated each limit as a band, where the lower limit is the 7 TeV value and the upper limit is the same value scaled linearly to 4 TeV. The real damage limit is somewhere in between and probably closer to the lower limit. Furthermore, our simulations suggest that smaller fractions of up to about 10 bunches may impact, instead of a single one. This causes an uncertainty on the damage level, which should in the future be updated for more realistic impact distributions and including the time delays between the bunches.

Another uncertainty comes from the fact that the damage levels are likely higher for the cases dominated by secondary halo, in particular the TCT in IR5, B2. The reason is that the secondary halo is much more spread out than a nominal beam, due to the scattering in the TCS6.

Therefore, this TCT should be further away from the damage limit than shown in Fig. 7.

The variation of the TCT setting in Fig. 7 can be seen as the combined effect of all errors altering the hierarchy, in particular orbit and beta beat. However, betatron phase errors cannot be consistently accounted for in this model and we therefore study this error separately. Imperfect phases are extracted from 1000 optics configurations with random magnetic errors, sampled with MAD-X, where the errors were tuned to produce a $\beta$-beat of about 10%. This is on the pessimistic side of what was obtained in the LHC [45,46].

With each imperfect phase configuration, we study the losses on the most critical TCT (IR1 B1). In the nominal optics with $\beta^* = 60$ cm, the fractional phase advance between the MKDs and the TCT is 57°, and the imperfections introduce a spread around this value with a standard deviation of 4° and a maximum, over 1000 seeds, of 13°. To save computing time and make significant statistics feasible, PSI is used, as the studied losses are primary, and the IR7 contribution is neglected.

The results are shown in Fig. 8, in the form of a probability distribution around the result for the perfect machine. The probabilities are calculated independently for each TCT setting. As can be seen, a very important variation in the losses is introduced by the phase errors, which can change the number of impacts by more than an order of magnitude compared to the perfect phase. With the TCT at the TCDQ position, which in itself should have a probability of 1% or below according to previous calculations, the probability on top of this for any kind of damage is less than 1%, and catastrophic damage is at permil level. Thus, the numerical simulations presented in Figs. 7–8 confirm that the 2012 collimator settings are safe within the postulated statistical limit.

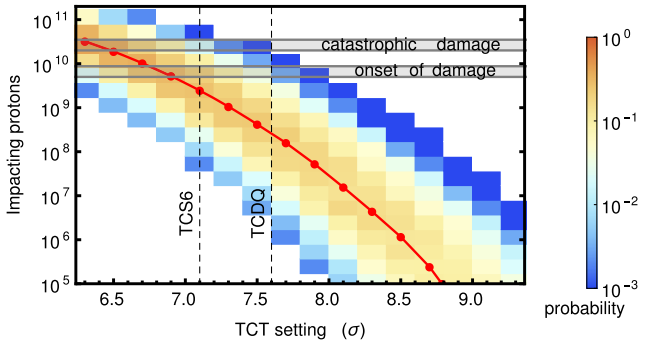


FIG. 8. The simulated losses during a single-module prefire from PSI on the TCT in IR1, B1, when all IR7 collimators are retracted, as a function of TCT setting. The solid red curve shows the result for a perfect optics, while the color scale shows, for each TCT setting, the probability distribution of losses under the influence of random phase errors compatible with the LHC optics correction. The results are shown together with the TCT damage limits given in Ref. [28].

## VIII. OUTLOOK FOR RUN II

In 2013, the LHC was shut down for work that will allow operation at a higher energy [69] and the restart at 6.5 TeV is, at the time of writing in 2015, underway. Operation will start at the relatively relaxed $\beta^* = 80$ cm [70,71], based on the $\beta^*$-reach established [56] using the methods from Secs. IV–VI, in order to have extra margins at the beginning of the run. This $\beta^*$-value can be decreased later, when the beam and machine behavior at higher energy and intensity is better known, in particularly in terms of impedance [72] and beam-beam effects [58], and after reestablishing safe operation in the 100 MJ regime. Under optimistic assumptions, even $\beta^* = 40$ cm could be within reach, which is significantly below the nominal 55 cm. The final limit will be calculated based on the initial beam experience.

Some improvements to the collimation margins could be envisaged in Run II. During the shutdown, the TCTs and the IR6 TCSGs were upgraded with integrated BPMs [34,73–75]. A newly developed temperature-insensitive electronics allows us to determine if parts of the observed drifts in Run I were an artifact caused by the temperature dependence of the present BPMs. Furthermore, interlocks could dump the beam if the margin between the dump protection and the TCTs goes below a certain threshold. The BPMs allow also a very fast alignment, which could even be done online to compensate for drifts. These improvements could allow for a reduction of the orbit margins and hence an improved reach in $\beta^*$.

Furthermore, Fig. 8 shows that the TCT hits during a SMPF or AD depend strongly on the phase advance from the MKDs. If it could be matched further away from 90°, the TCT impacts could be significantly reduced and, potentially, also the collimation hierarchy margins. The TCT settings could then be determined based on the expected impacts and the damage limit, with a suitable error margin. This would mean abandoning the pessimistic assumption of a 90° phase advance. Such a model could profit also from improved estimates of the damage limit, taking into account more realistic beam distributions than previously.

## IX. CONCLUSIONS

The LHC stores dangerous beams that could seriously damage the accelerator. This couples collimation to the luminosity performance. When $\beta^*$ is reduced, so is the available aperture in the inner triplets, which have to be protected by the collimators. Therefore, the collimator settings directly limit the reach in $\beta^*$.

We have presented a calculation model to determine optimized collimator settings that provide adequate protection without unnecessarily large margins and therefore improve the reach in $\beta^*$. The model was used to determine the collimator settings in the 2011–2012 LHC physics runs.

The tighter collimator settings, together with aperture measurements and a tighter beam-beam separation, allowed a reduction of $\beta^*$ in steps from 3.5 m in 2010 to 0.6 m in 2012. Compared to the conservative approach taken in 2010, the application of the presented calculation model for collimator settings gave the largest gain (a factor 2.3 in $\beta^*$) and allowed more than a factor 2 higher luminosity. The use of realistic aperture estimates, based on measurements, was almost as important (a factor 1.7 in $\beta^*$). These two contributions were essential to the success and discoveries of the LHC in Run I.

In Run II, further performance improvements based on even tighter collimator settings could be envisaged. In particular, the use of new integrated BPM buttons or a favorable phase advance between the beam dump kickers and sensitive elements could allow reducing the margins between collimators. The final reach in $\beta^*$ has, however, to be established based on initial beam tests and operation at higher energy in an initial relaxed configuration.

Our results show the importance of the collimation hierarchy in high-energy colliders and its direct influence on luminosity. This serves as an important input for future machines with dangerous beams, such as the HL-LHC or the FCC, where the collimator settings can be determined by adapting our calculations. Furthermore, the impact on luminosity from the machine protection constraints could be minimized by designing the optics such that the phase advance between extraction kickers and sensitive equipment is favorable, choosing more robust collimator materials, or improving the reliability of the beam extraction system.

## ACKNOWLEDGMENTS

We would like to thank several colleagues for helpful input and discussions: G. Arduini, A. Bertarelli, C. Bracco, F. Carra, R. De Maria, S. Fartoukh, M. Giovannozzi, B. Goddard, W. Herr, M. Lamont, L. Lari, T. Pieloni, R. Tomas, J. Uythoven, G. Vanbavinckhove, J. Wenninger, D. Wollmann, and M. Zerlauth.

## APPENDIX A: ABBREVIATIONS

We summarize below, in alphabetical order, all abbreviations used throughout the paper.

AD: asynchronous dump

B1, B2: the two counterrotating beams in the LHC

BLM: beam loss monitor

BPM: beam position monitor

CFC: carbon-fiber composite

FCC: Future Circular Collider

HL-LHC: High-Luminosity Large Hadron Collider (a future upgrade of the LHC under study) [15]

IP: interaction point

IR: insertion region. The LHC has eight IRs. The experiments are located in IR1. IR2. IR5, and IR8. The main part of the collimation system is found in IR3 and IR7 and the beam extraction system is located in IR6.

LHC: Large Hadron Collider [1,2]

MB: main bending magnet

MKD: extraction kicker magnet in the beam dumping system

PSI: phase-space integration

QF: focusing quadrupole

QD: defocusing quadrupole

TCP7: primary betatron collimator in IR7

TCS7: secondary betatron collimator in IR7

TCLA7: absorber in IR7

TCTH, TCTV: horizontal (H) or vertical (V) tertiary collimator located in the experimental insertions

TCS6: secondary collimator used for beam dump protection in IR6

TCDQ: large absorber used for beam dump protection in IR6

SMPF: single-module prefire

## APPENDIX B: CORRELATED ORBIT MARGIN

We derive here the reduction in margin due to correlated orbit movements between a TCT and the aperture of the closest triplet (upstream of the IP), for which we use the subscripts 1 and 2. The phase advance between the TCT and the aperture bottleneck on the incoming beam is only about 4°, so that we with good approximation can consider that any particle has the same amplitude in $\sigma$ and the same sign at the two locations, which significantly simplifies the calculations. The small phase advance can be understood from the large $\beta$-function in the insertion, which is necessary to focus down to a small $\beta^*$ (see Fig. 1).

We consider the situation illustrated schematically in Fig. 9. During the qualification of the protection, right after the alignment, we assume that the TCT is centered at a distance $A_1$ (in units of $\sigma$) around the reference orbit, while the unmovable triplet aperture $A_2$ is centered around the

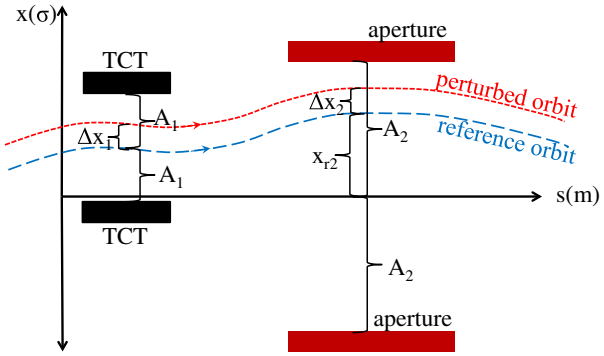


FIG. 9. A schematic view of a collimator protecting an aperture illustrating the variables introduced in Appendix B. The collimator is initially centered around the reference orbit, which is present during the collimation setup. At a later time, the orbit can be slightly perturbed.

zero orbit. The aperture margin is thus $A_1$ in the TCTs and $A_2 \pm x_{r2}$ in the triplet, where $x_{r2}$ is the triplet reference orbit in the relevant plane ($-$ for the side where the $x$ is defined positive, $+$ on the other side). The retraction between triplet and TCT is thus $A_2 \pm x_{r2} - A_1$, meaning that the minimum margin $M_{\mathrm{min}}$ over the two sides, with all quantities in units of $\sigma$, is

$$M_{\mathrm{min}} = \min\{A_2 - x_{r2} - A_1, A_2 + x_{r2} - A_1\} = A_2 - A_1 - |x_{r2}|. \quad \text{(B1)}$$

We assume that this configuration has been successfully qualified and consider now a later time where the orbit has drifted by $\Delta x_1$ at the TCT and $\Delta x_2$ at the triplet. If $\Delta x_1 > 0$, there is an *increase* in retraction to the triplet on the positive side and a *decrease* on the negative side. On the other hand, $\Delta x_2 > 0$ means *decreased* margin on the positive side. The new margin therefore becomes $A_2 - (x_{r2} + \Delta x_2) - (A_1 - \Delta x_1)$ and $A_2 + (x_{r2} + \Delta x_2) - (A_1 + \Delta x_1)$ on the negative side. The new minimum margin becomes

$$\tilde{M}_{\mathrm{min}} = \min\{A_2 - (x_{r2} + \Delta x_2) - (A_1 - \Delta x_1), A_2 + (x_{r2} + \Delta x_2) - (A_1 + \Delta x_1)\} = A_2 - A_1 - |x_{r2} + \Delta x_2 - \Delta x_1|. \quad \text{(B2)}$$

The change in the minimum margin with respect to the qualification is

$$\Delta M_{\mathrm{orbit}} = \tilde{M}_{\mathrm{min}} - M_{\mathrm{min}} = |x_{r2}| - |x_{r2} + \Delta x_2 - \Delta x_1|. \quad \text{(B3)}$$

In this calculation, we assume that a TCT jaw protects the triplet aperture on the same side, as is the case for the closest triplet (phase advance $\Delta\mu \approx 0$). At the other triplet downstream of the IP (see Fig. 1), a TCT jaw protects the opposite side since $\Delta\mu \approx \pi$. This changes the sign of $\Delta x_1$ in Eq. (B3). The maximum change in margin, over both sides and both the triplets on both sides of the IP, is thus smaller than

$$\Delta M_{\mathrm{orbit}} = |x_{r2}| - |x_{r2} + \Delta x_2 + |\Delta x_1||. \quad \text{(B4)}$$

We can also calculate the correlated margin between two collimators, where the orbit is initially centered at both devices. We set then $x_{r2} = 0$ in Eq. (B4) and introduce the absolute value on $|\Delta x_2|$. If $x_{r2} = 0$, any change in orbit causes a reduction in margin, while if $x_{r2} \neq 0$, the margin could also increase. It should be noted that the correlated treatment of the orbit movements between the dump protection and the TCTs results in the same margin as the uncorrelated treatment shown in Eq. (3).

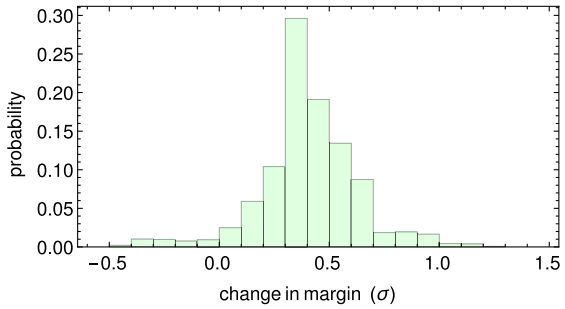


FIG. 10. Change of margin due to orbit movements between the horizontal TCT in IR5 B2 and the aperture bottleneck in triplet (bottom) as calculated by Eq. (B4). All running periods from 2011 with stable beams and $\beta^* = 1$ m were accounted for, except where large luminosity scans were performed. The orbits were sampled every 10 s.

An example of the measured distribution of $\Delta M_{\mathrm{orbit}}$ during the 2011 run is shown in Fig. 10. Just as for the orbit at individual elements, as in Fig. 4, significant deviations of seemingly random nature are observed.

[1] L. Evans and P. Bryant, LHC machine, JINST **3**, S08001 (2008).
[2] O. S. Brüning, P. Collier, P. Lebrun, S. Myers, R. Ostojic, J. Poole, and P. Proudlock, Report No. CERN-2004-003-V1, 2004.
[3] *Handbook of Accelerator Physics and Engineering*, edited by A. W. Chao and M. Tigner (World Scientific, Singapore, 1998).
[4] At very small $\beta^*$, $F$ is more important and causes a significant loss in $\mathcal{L}$, however, $\mathcal{L}$ always increases when $\beta^*$ is decreased.
[5] R. de Maria, General method for final focus system design for circular colliders, Phys. Rev. ST Accel. Beams **11**, 031001 (2008).
[6] LHC optics web, http://lhc-optics.web.cern.ch/lhc-optics/www/.
[7] MAD-X program, http://cern.ch/mad/.
[8] J. B. Jeanneret, Optics of a two-stage collimation system, Phys. Rev. ST Accel. Beams **1**, 081001 (1998).
[9] R. W. Assmann, in *Proceedings of the LHC Project Workshop - Chamonix XIV, Chamonix, France* (CERN, Geneva, 2005), p. 261.
[10] G. Robert-Demolaize, Ph.D. thesis, Universite Joseph Fourier, Grenoble, 2006.
[11] R. W. Assmann *et al.*, in *Proceedings of the 10th European Particle Accelerator Conference, Edinburgh, Scotland, 2006* (EPS-AG, Edinburgh, Scotland, 2006), p. 986.
[12] C. Bracco, Ph.D. thesis, EPFL Lausanne, 2008.
[13] D. Wollmann *et al.*, in *Proceedings of the International Particle Accelerator Conference, Kyoto, Japan* (ICR, Kyoto, 2010), p. 1237.
[14] R. W. Assmann, in *Proceedings of the LHC Performance Workshop, Chamonix XII* (CERN, Geneva, 2003).

[15] L. Rossi, in *Proceedings of the 2nd International Particle Accelerator Conference, San Sebastiáán, Spain* (EPS-AG, Spain, 2011).

[16] F. Zimmermann, M. Benedikt, D. Schulte, and J. Wenninger, in *Proceedings of the International Particle Accelerator Conference 2014, Dresden, Germany* (EPS-AG, Dresden, 2014), p. 1.

[17] R. Bruce, R. W. Assmann, V. Boccone, G. Bregliozzi, H. Burkhardt, F. Cerutti, A. Ferrari, M. Huhtinen, A. Lechner, Y. Levinsen, A. Mereghetti, N. V. Mokhov, I. S. Tropin, and V. Vlachoudis, Sources of machine-induced background in the ATLAS and CMS detectors at the CERN Large Hadron Collider, Nucl. Instrum. Methods Phys. Res., Sect. A **729**, 825 (2013).

[18] C. Alabau Pons, R. Assmann, R. Bruce, M. Giovannozzi, E. MacLean, G. Mueller, S. Redaelli, F. Schmidt, R. Tomas, and J. Wenninger, CERN-ATS Report No. Note-2011-110 MD, 2011.

[19] R. Bruce, R. de Maria, S. Fartoukh, M. Giovannozzi, S. Redaelli, R. Tomas, and J. Wenninger, CERN Report No. CERN-ACC-2014-0044, 2014.

[20] S. Redaelli *et al.*, Overview of aperture measurements at the CERN Large Hadron Collider (LHC) (to be published).

[21] W. Herr, M. Albert, R. Alemany, R. Assmann, X. Buffat, R. Calaga, K. Cornelis, M. Fitterer, R. Giachino, R. Miyamoto, L. Norman, G. Papotti, T. Pieloni, L. Ponce, S. Redaelli, M. Schaumann, G. Trad, and D. Wollmann, CERN-ATS Report No. 2011-058 MD, 2011.

[22] W. Herr, R. Alemany, R. Assmann, X. Buffat, R. Calaga, M. Fitterer, G. H. Hemelsoet, R. Giachino, G. Papotti, T. Pieloni, M. Poyer, G. Trad, M. Schaumann, and D. Wollmann, CERN-ATS Report No. 2011-120 MD, 2011.

[23] R. Assmann, R. Bruce, M. Giovannozzi, M. Lamont, E. Maclean, R. Miyamoto, G. Mueller, G. Papotti, L. Ponce, S Redaelli, and J. Wenninger, CERN-ATS Report No. 2012-005 MD, 2012.

[24] R. Bruce and R. W. Assmann, in *Proceedings of the 2011 LHC beam operation workshop, Evian, France* (CERN, Geneva, 2011).

[25] E. B. Holzer, B. Dehning, E. Effinger, J. Emery, G. Ferioli, J. L. Gonzalez, E. Gschwendtner, G. Guaglio, M. Hodgson, D. Kramer, R. Leitner, L. Ponce, V. Prieto, M. Stockner, and C. Zamantzas, Beam loss monitoring system for the LHC, IEEE Nuclear Science Symposium Conference Record **2**, 1052 (2005).

[26] E. B. Holzer *et al.*, in *Proceedings of the 11th European Particle Accelerator Conference, Genoa, 2008* (EPS-AG, Genoa, Italy, 2008), p. 1134.

[27] For skew collimators at an angle $\vartheta$ in the transverse plane, with beam sizes $\sigma_x$ and $\sigma_y$ in the horizontal and vertical planes, we use the skew beam size $\sigma = \sqrt{\sigma_x^2 \cos^2\vartheta + \sigma_y^2 \sin^2\vartheta}$.

[28] A. Bertarelli *et al.*, in *MPP Workshop March 2013, Annecy, France* (CERN, Geneva, 2013).

[29] R. W. Assmann, B. Goddard, E. Vossenberg, and E. Weisse, LHC Project Report No. 293, 1996.

[30] R. Schmidt, R. Assmann, E. Carlier, B. Dehning, R. Denz, B. Goddard, E. B. Holzer, V. Kain, B. Puccio, B. Todd, J. Uythoven, J. Wenninger, and M. Zerlauth, *Protection of the CERN Large Hadron Collider*, *New J. Phys.* 8, 290 (2006).

[31] T. Kramer, Ph.D. thesis, TU Graz, 2008.

[32] W. Weterings, B. Goddard, B. Riffaud, and M. Sans Merce, in *Proceedings of the 9th European Particle Accelerator Conference, Lucerne, 2004* (EPS-AG, Lucerne, 2004), p. 629 [http://accelconf.web.cern.ch/AccelConf/e04/].

[33] G. Valentino, R. Aßmann, R. Bruce, S. Redaelli, A. Rossi, N. Sammut, and D. Wollmann, Semiautomatic beam-based LHC collimator alignment, Phys. Rev. ST Accel. Beams **15**, 051002 (2012).

[34] G. Valentino, A. A. Nosych, R. Bruce, M. Gasior, D. Mirarchi, S. Redaelli, B. Salvachua, and D. Wollmann, Successive approximation algorithm for beam-position-monitor-based LHC collimator alignment, Phys. Rev. ST Accel. Beams **17**, 021005 (2014).

[35] N. Mounet *et al.*, in *LHC Collimation Review 2013* (CERN, Geneva, 2013).

[36] R. Bruce, R. W. Assmann, and S. Redaelli, in *Proceedings of the 2nd International Particle Accelerator Conference, San Sebastiáán, Spain* (EPS-AG, Spain, 2011), p. 3753.

[37] R. W. Assmann, R. Bruce, F. Burkart, M. Cauchi, D. Deboy, L. Lari, E. Metral, N. Mounet, S. Redaelli, A. Rossi, B. Salvant, G. Valentino, and D. Wollmann, CERN-ATS Report No. 2011-036 MD, 2011.

[38] R. W. Assmann, R. Bruce, F. Burkart, M. Cauchi, D. Deboy, L. Lari, S. Redaelli, A. Rossi, G. Valentino, and D. Wollmann, CERN-ATS Report No. 2011-079 MD, 2011.

[39] R. W. Assmann, R. Bruce, F. Burkart, M. Cauchi, D. Deboy, L. Lari, S. Redaelli, A. Rossi, B. Salvachua, G. Valentino, and D. Wollmann, CERN-ATS Report No. 2012-022 MD, 2012.

[40] R. W. Assmann, R. Bruce, F. Burkart, M. Cauchi, D. Deboy, S. Redaelli, R. Schmidt, A. Rossi, G. Valentino, and D. Wollmann, CERN-ATS Report No. 2011-125 MD, 2011.

[41] N. Mounet, E. Metral, G. Arduini, T. Pieloni, B. Salvant, S. White, X. Buffat, R. Calaga, J. Esteban-Muller, R. Bruce, S. Redaelli, B. Salvachua, and G. Rumolo, in *Proceedings of the 2012 LHC beam operation workshop, Evian, France* (CERN, Geneva, 2012).

[42] T. Pieloni, X. Buffat, S. White, N. Mounet, W. Herr, E. Metral, G. Arduini, and R. Bruce, in *Proceedings of the 2012 LHC beam operation workshop, Evian, France* (CERN, Geneva, 2012).

[43] R. Bruce and R. W. Assmann, in *Proceedings of the 2010 LHC beam operation workshop, Evian, France (CERN, Geneva, 2010), p. 133.*

[44] R. Tomás, O. Brüning, M. Giovannozzi, P. Hagen, M. Lamont, F. Schmidt, G. Vanbavinckhove, M. Aiba, R. Calaga, and R. Miyamoto, Cern large hadron collider optics model, measurements, and corrections, Phys. Rev. ST Accel. Beams **13**, 121004 (2010).

[45] G. Vanbavinckhove, M. Aiba, R. Calaga, R. Miyamoto, and R. Tomas, in *Proceedings of the 2nd International Particle Accelerator Conference, San Sebastiáán, Spain* (EPS-AG, Spain, 2011), p. 2061.

[46] R. Tomás, T. Bach, R. Calaga, A. Langner, Y. I. Levinsen, E. H. Maclean, T. H. B. Persson, P. K. Skowronski, M.

Strzelczyk, G. Vanbavinckhove, and R. Miyamoto, Record low $\beta$ beating in the lhc, Phys. Rev. ST Accel. Beams **15**, 091001 (2012).
[47] T. Baer, K. Fuchsberger, R. Schmidt, and J. Wenninger, in *Proceedings of the 3rd International Particle Accelerator Conference, New Orleans, LA, 2012* (IEEE, Piscataway, NJ, 2012), p. 3746.
[48] J. B. Jeanneret and T. Risselada, LHC Project Report No. 66, 1996.
[49] J. B. Jeanneret and R. Ostojic, LHC Project Report No. 111, 1997.
[50] C. Alabau Pons, M. Giovannozzi, G. Müller, S. Redaelli, F. Schmidt, R. Tomas, and J. Wenninger, in *Proceedings of the International Particle Accelerator Conference, Kyoto, Japan* (ICR, Kyoto, 2010), p. 477.
[51] R. W. Assmann, R. Bruce, M. del Carmen Alabau, M. Giovannozzi, G. J. Mueller, S. Redaelli, F. Schmidt, R. Tomas, J. Wenninger, and D. Wollmann, in *Proceedings of the 2nd International Particle Accelerator Conference, San Sebastiáán, Spain* (EPS-AG, Spain, 2011), p. 1810.
[52] S. Redaelli, C. Alabau Pons, R. Assmann, R. Bruce, M. Giovannozzi, G. Muller, M. Pojer, and J. Wenninger, in *Proceedings of the 3rd International Particle Accelerator Conference, New Orleans, LA, 2012* (IEEE, Piscataway, NJ, 2012), p. 508.
[53] C. Alabau Pons, A. Arduini, R. W. Assmann, R. Bruce, M. Giovannozzi, J. M. Jowett, E. MacLean, G. Muller, S. Redaelli, R. Tomas, G. Valentino, and J. Wenninger, CERN-ATS Report No. 2012-017 MD, 2012.
[54] R. Bruce, M. Giovannozzi, P. D. Hermes, B. Holzer, A. A. Nosych, S. Redaelli, and J. Wenninger, CERN-ATS Report No. 2013-026 MD, 2013.
[55] R. Bruce, M. Giovannozzi, P. D. Hermes, S. Redaelli, and J. Wenninger, CERN-ACC Report No. 2013-0011 MD, 2013.
[56] R. Bruce and S. Redaelli, in *Proceedings of the 5th Evian Workshop, Evian, France* (CERN, Geneva, 2014).
[57] W. Herr, X. Buffat, R. Calaga, R. Giachino, D. Kaltchev, G. Papotti, and T. Pieloni, in *Proceedings of the ICFA Mini-Workshop on BeamBeam Effects in Hadron Colliders, CERN, Geneva, Switzerland, March 2013* (CERN, Geneva, 2013), p. 1822.
[58] T. Pieloni, X. Buffat, D. Banfi, J. Barranco, G. Arduini, E. Metral, N. Mounet, S. M. White, and J. Qiang, in *Proceedings of the 5th Evian Workshop, Evian, France* (CERN, Geneva, 2014).
[59] R. Bruce, D. Bocian, S. Gilardoni, and J. M. Jowett, Beam losses from ultraperipheral nuclear collisions between Pb ions in the Large Hadron Collider and their alleviation, Phys. Rev. ST Accel. Beams **12**, 071002 (2009).
[60] http://www.wolfram.com.
[61] F. Schmidt, Report No. CERN/SL/94-56-AP, 1994.
[62] G. Robert-Demolaize, R. Assmann, S. Redaelli, and F. Schmidt, in *Proceedings of the 21st Particle Accelerator Conference, Knoxville, TN, 2005* (IEEE, Piscataway, NJ, 2005), p. 4084.
[63] C. Tambasco, Master's thesis, Università di Roma, Italy, 2014.
[64] C. Tambasco *et al.*, Improved physics model for collimation tracking studies at LHC (to be published).
[65] R. Bruce, R. W. Assmann, V. Boccone, C. Bracco, M. Brugger, M. Cauchi, F. Cerutti, D. Deboy, A. Ferrari, L. Lari, A. Marsili, A. Mereghetti, D. Mirarchi, E. Quaranta, S. Redaelli, G. Robert-Demolaize, A. Rossi, B. Salvachua, E. Skordis, C. Tambasco, G. Valentino, T. Weiler, V. Vlachoudis, and D. Wollmann, Simulations and measurements of beam loss patterns at the CERN Large Hadron Collider, Phys. Rev. ST Accel. Beams **17**, 081004 (2014).
[66] L. Lari *et al.*, in *Proceedings of the 3rd International Particle Accelerator Conference, New Orleans, LA, 2012* (IEEE, Piscataway, NJ, 2012), p. 547.
[67] L. Lari, C. Bracco, R. Bruce, B. Goddard, S. Redaelli, B. Salvachua, G. Valentino, and A. Faus-Golfe, in *Proceedings of the 4th International Particle Accelerator Conference, IPAC-2013, Shanghai, China, 2013* (JACoW, Shanghai, China, 2013), p. 996.
[68] B. Goddard (private communication).
[69] K. Foraz, in *Proceedings of the LHC Performance Workshop (Chamonix 2012)* (CERN, Geneva, 2012).
[70] LHC Machine Committee, September 3 2014, https://indico.cern.ch/event/337929/.
[71] R. Bruce, G. Arduini, S. Fartoukh, M. Giovannozzi, M. Lamont, E. Metral, T. Pieloni, S. Redaelli, and J. Wenninger, in *Proceedings of the LHC Performance Workshop (Chamonix 2014), Chamonix, France* (CERN, Geneva, 2014).
[72] N. Mounet, R. Bruce, X. Buffat, T. Pieloni, B. Salvant, and E. Metral, in *Proceedings of the 5th Evian Workshop, Evian, France* (CERN, Geneva, 2014).
[73] B. Salvachua, G. Valentino, O. Aberle, J. Albertone, S. Athanasiadis, V. Baglin, A. Bertarelli, C. Boccard, R. Bruce, F. Carra, G. Cattenoz, J. Coupard, S. Chemli, C. Derrez, L. Esposito, R. Folch, I. Lamas, J. Lendaro, R. Losito, A. Marsili, A. Masi, D. Mirarchi, E. Quaranta, S. Redaelli, A. Rossi, and I. Sexton, in *Proceedings of the 5th Evian Workshop, Evian, France* (CERN, Geneva, 2014).
[74] D. Wollmann, A. A. Nosych, G. Valentino, O. Aberle, R. W. Assmann, A. Bertarelli, C. Boccard, R. Bruce, F. Burkart, E. Calvo, M. Cauchi, A. Dallocchio, D. Deboy, M. Gasior, R. Jones, V. Kain, L. Lari, S. Redaelli, and A. Rossi, Beam feasibility study of a collimator with in-jaw beam position monitors, Nucl. Instrum. Methods Phys. Res., Sect. A **768**, 62 (2014).
[75] S. Redaelli *et al.*, The run ii LHC: collimation system (to be published).